Multifunctional Properties of Polyvinylidene-Fluoride-Based Materials: From Energy Harvesting to Energy Storage

Matthieu Fricaudet, Katarina Žiberna, Samir Salmanov, Jens Kreisel, Delong He, Brahim Dkhil, Tadej Rojac, Mojca Otoničar, P.-E. Janolin, Andraž Bradeško

To cite this version:

Matthieu Fricaudet, Katarina Žiberna, Samir Salmanov, Jens Kreisel, Delong He, et al.. Multifunctional Properties of Polyvinylidene-Fluoride-Based Materials: From Energy Harvesting to Energy Storage. ACS Applied Electronic Materials, 2022, 4 (11), pp.5429-5436. 10.1021/acsaelm.2c01091 . hal-03903248

HAL Id: hal-03903248

https://centralesupelec.hal.science/hal-03903248v1

Submitted on 16 Dec 2022

Multifunctional properties of polyvinylidene-fluoride-based materials: from energy harvesting to energy storage

Matthieu Fricaudet[1]*, *Katarina Žiberna*[2], *Samir Salmanov*[2], *Jens Kreisel*[3], *Delong He*[4], *Brahim Dkhil*[1], *Tadej Rojac*[2], *Mojca Otoničar*[2], *Pierre-Eymeric Janolin*[1], *Andraž Bradeško*[1]

[1]Université Paris-Saclay, CNRS, CentraleSupélec, Laboratoire SPMS, 91190 Gif-sur-Yvette, France

[2]Jožef Stefan Institute, Jamova cesta 39, 1000 Ljubljana, Slovenia

[3]Department of Physics and Materials Science, University of Luxembourg, and Materials Research and Technology Department, Luxembourg Institute of Science and Technology, L-4422 Belvaux, Luxembourg.

[4]Université Paris-Saclay, CNRS, CentraleSupélec-ENS Paris-Saclay, Laboratoire LMPS, 91190 Gif-sur-Yvette, France

*matthieu.fricaudet@centralesupelec.fr

Abstract

Organic ferroelectrics are increasingly important due to their complementary properties to classical, inorganic ferroelectrics. Flexibility, chemical resistance, scalability, high breakdown fields, and biocompatibility are attractive for many applications like energy harvesting and storage. The most known energy harvesting methods are piezoelectric, pyroelectric, and triboelectric. Here, we apply the well-established material's figures of merit to five polyvinylidene-fluoride-based compositions ranging from ferroelectric to relaxor-like behavior to emphasize the importance of several key material parameters contributing to the maximal power output of energy harvesting devices. Afterward, we discuss the possibility of the same functional material storing the output energy for the development of scalable multifunctional devices.

Keywords: Energy harvesting, PVDF, piezoelectricity, pyroelectricity, triboelectricity, energy storage

1. Introduction

Ferroelectrics and their energy conversion ability are utterly crucial for various applications in modern electronics. The most common ferroelectric materials are inorganic oxides in single crystal or ceramic form [1].

In recent years, the need to develop flexible electronics has emerged due to the increased popularity of body-worn devices in all aspects of our life [2,3]. This raised the need for materials that can be fabricated on flexible substrates, scalable, withstand wear and temperature variations, and are chemically resistant and biocompatible. Organic ferroelectrics, especially polyvinylidene-fluoride-(PVDF)-based materials, proved suitable for such applications [4]. PVDF-based materials range from classical ferroelectric-like behavior to the relaxor-like, depending on the chemical composition or treatment [5–7]. This versatility uncovers opportunities to integrate these flexible materials to various applications, from electrocaloric cooling [8] and neuromorphic computing [9] to different actuation [10], sensing [11], and energy harvesting technologies [12].

The leading energy harvesting technologies in organic ferroelectrics are designed to exploit piezoelectricity, pyroelectricity, and triboelectricity. Piezoelectric energy harvesting benefits from the piezoelectric response, generating charges under applied mechanical stress. The piezoelectric effect converts mechanical vibrations into useful electrical energy [13]. The pyroelectric effect is, by definition, a change of the surface charge under varying temperatures [14,15]. Latest studies show this effect can power simple electronic circuits by converting the energy from the finger touch and chemical reactions to electricity [16]. For both these effects, organic ferroelectric benefit from their low dielectric constant, which allows them to compensate for their relatively smaller pyroelectric and piezoelectric constants compared to inorganics materials and gives them competitive harvesting capabilities. Recently, the triboelectric effect has shown great promise due to the relative simplicity and large power output demonstrated [17]. In principle, the triboelectric effect is the generation of surface charge upon contacting two surfaces and the corresponding electrical work (electrostatic induction) to compensate for the formed surface charges.

In the next stage of the harvesting process, the electrical energy must be efficiently manipulated by energy reclamation circuits and stored in a medium [18,19]. Surprisingly, organic ferroelectrics are also prominent candidates for energy storage, especially some PVDF-based compositions [20,21].

Until now, many research articles have been published on energy harvesting and energy storage with PVDF-based materials. However, there were no systematic investigations to uncover the good practices in the selection process for the optimal PVDF-based material within the poly(vinylidene fluoride-trifluoroethylene-chlorofluoroethylene) (P(VDF-TrFE-CFE)) system for a given energy harvesting application [10,22]. Furthermore, the emerging idea is to combine several stages of energy harvesting within one material to make compact, scalable devices [23].

Here, we illustrate the multifunctionality of PVDF-based polymers with different amounts of trifluoroethylene (TrFE) and chlorofluoroethylene (CFE) co- and ter- polymers, respectively. We focus on the energy conversion aspect at room temperature. A benchmarking investigation is made to determine which compositions are optimal for specific energy harvesting methods. The thick films used in this study were prepared by the solution casting method and their electric, electromechanical, pyroelectric, and triboelectric properties are presented herein. After illustrating the energy generation aspect of these multifunctional materials, we show that they can also be used to store the harvested energy. Finally, the optimal composition as the best all-in-one material for efficient harvesting of energy from all possible sources and its efficient storage is pointed out and discussed.

2. Experimental section

The polymers in the form of powders were obtained from Piezotech-Arkema, France. The composition of powders and notations used in this paper are given in Table 1. These PVDF-based compositions are the most investigated and reported ones. The powders were dissolved in the dimethylformamide solution (99.8 %, Alfa Aesar, Germany) in the weight ratio of 20 % and mixed for 2h at ~60 °C. The deposition was done by solvent casting (Elcometer 4340, United Kingdom), with the speed of the blade (Elcometer 3580/7, United Kingdom) and its height adjusted to get uniform ~30 μm thick films. The temperature of the glass substrate was set to 55 °C. The films were dried at 55 °C for 1 hour, then removed from the substrate and finally annealed at 120 °C for 50 min. For electrical measurements 50-nm-Au electrodes were deposited on both sides by magnetron sputtering (MP300, PLASSYS, France).

X-ray data collection was performed by a homemade diffractometer (radius = 500 mm) associated with a Rigaku RA-HF18 rotating anode generator (50 kV, 200mA). The wavelength was copper Kα radiation (0.1541 nm), and the step was 0.02°. The microstructures of the surfaces of the polymer films were investigated using a field-emission scanning electron microscope (SEM) Verios 4G HP (Thermo Fischer, Waltham, Massachusetts, USA), operated in secondary electron emission mode at 2 keV. To ensure sample surface conductivity and avoid charging during SEM imaging, the samples were coated with 5 nm of carbon using a Precision Etching and Coating System 628A (Gatan, Pleasanton, California, USA).

Electrical measurements were performed by an impedance meter (Agilent 4294, CA, USA). A parallel RC circuit was used to calculate the dielectric permittivity of the samples in the temperature range from room temperature to 140 °C. The samples were poled at 1 MV/cm

(Keithley 248, CLE, USA) for 10 min at room temperature. The direct piezoelectric response was measured on the Berlincourt-type piezometer (PM10, Piezotest, Singapore) under 20 Hz sinusoidal force excitation. Polarization loops were measured using a piezoelectric testing equipment (TF-2000, Aixacct, Germany) at a frequency of 20 Hz and a magnitude of electric field of 1 MV/cm.

Pyroelectric response was measured on an Aixacct TF-2000 system with a pyroelectric module. The heating rate was 5 K/min, and the temperature variation amplitude was 20 K. A Fast Fourier transform (FFT) filter was used to reduce the noise level.

The triboelectric effect was measured in the contact-separation mode. One Au electrode of 2 cm diameter was sputtered on the sample face, while the other electrical contact was placed on a contacting aluminum plate. The excitation frequency was 15 Hz, the displacement was generated with a linear electromagnetic motor, and the waveform was sinusoidal. The force was measured with a force sensor. The generated triboelectric voltage was measured by a multimeter (Keithley 2700, CLE, USA) and an oscilloscope (Agilent DSO-X 2012A, CA, USA) in a series with a 100 MΩ resistor (to not affect the signal with the measurements input impedances).

Table 1. The chemical composition and the notation used (ref. datasheet).

Commercial name	VDF (wt %)	TrFE (wt %)	CFE (wt %)	Notation
FC20	79.6	20.4	/	80/20
FC25	75.1	24.9	/	75/25
FC30	70	30	/	70/30
FC45	54.5	45.5	/	55/45
FS-RS	64.6	26.2	9.2	CFE

3. Results and Discussion

3.1. Structural and microstructural properties

The structural properties of the samples were analyzed to ensure the fabrication and crystallization process was properly executed. Figure 1a shows the room temperature XRD pattern of the polymers. The PVDF-based polymers show only one clear peak in the 2Θ range from 16° to 21°. The slightly asymmetric Bragg peak corresponds to the (110) reflections of the all-trans (TTTT) molecular ferroelectric conformation (β-phase), i.e., all the dipoles in each (-CH_2–CF_2-)-like monomer are aligned along the same direction that is quasi-perpendicular to the polymer chain. No extra peak related to the non-polar (TGTG') α-phase could be evidenced. Note that Raman and IR spectroscopy measurements (not seen here) confirmed such results. The asymmetry of the left side of the peak comes from the presence of the (200) reflections [24]. With the increased amount of TrFE, the peaks shift to lower angles, and with the addition of CFE the shift is even more pronounced. This diffraction data were used to calculate the interchain spacing, which shows that the spacing increases with the addition of TrFE and CFE (Figure 1b). This is due to the partial substitution of the hydrogen (Van der Walls radius of r=1.20 Å) by the larger fluorine (r=1.47 Å), and even larger chlorine (r=1.75 Å) atoms in CFE, leading to the larger unit cell.

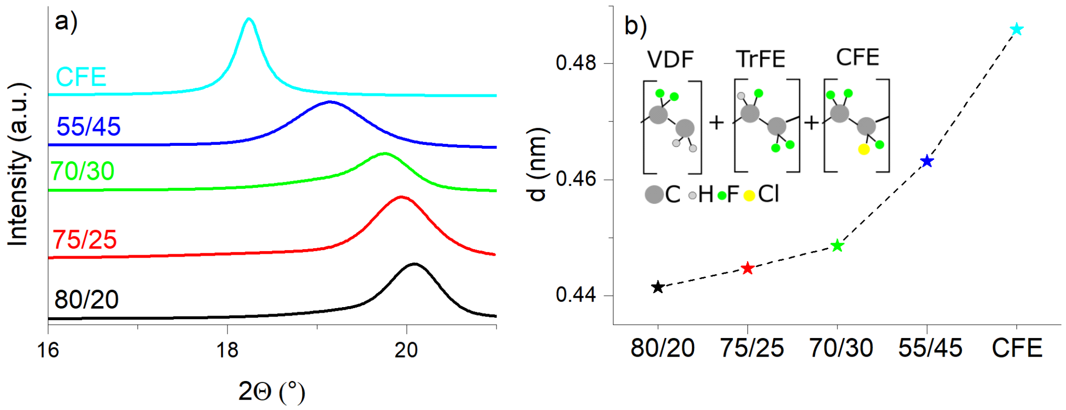

Figure 1. Structural analysis of the PVDF-based compositions. a) XRD patterns and b) interplanar spacing deduced from the Bragg peak positions. Note that here we only show the 2θ range where the Bragg peaks are the most intense while the diffraction pattern was measured between 10° to 60° in 2θ. The inset in b) schematically shows the chemistry of the VDF, TrFE and CFE monomers. Dashed line is a guide to the eye.

Figure 2 shows surface morphologies of the films with randomly oriented and intertwined needle-like or thread-like features which likely represent assemblies of ordered polymer chains and possibly reflect the level of film crystallinity. With the increasing amount of TrFE the anisotropy of the so-called threads slightly increases and then significantly increases in the case of the CFE ter-polymer. Indeed, for composition 80/20, the SEM image shows quite isotropic features with an average size of about 45 nm, while thread-like features are observed for all the other compositions with a diameter of ~35 nm that stays fixed while the length seems to continuously increase up to 1 micron with TrFE increasing. Besides the increased length of threads up to 1 micron, the addition of CFE reduces their intertwining and increases the distances between the threads. This suggests reduced inter-thread polar interactions that could lead to only short-range correlations which may explain the relaxor-like behavior of this composition.

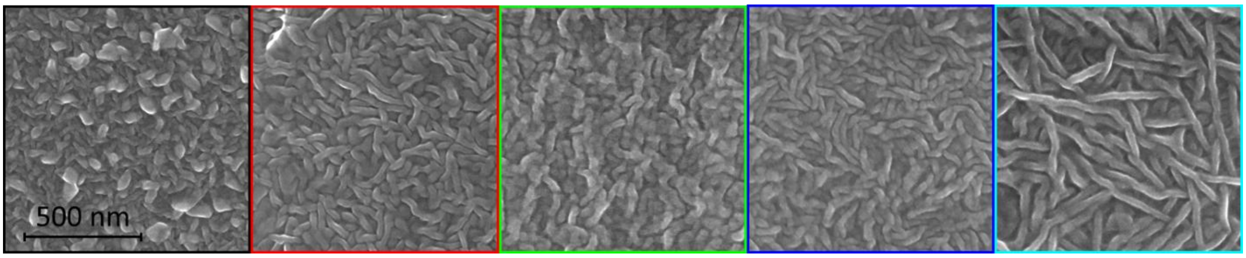

Figure 2. Microstructural images of the surface of 80/20, 75/25, 70/30, 55/45 and CFE polymer films. All images are at the same magnification.

3.2.Electrical response

The structural properties are reflected in the electrical response, as shown in Fig. 3. At first, the permittivity of the fabricated compositions was measured as a function of temperature. The peak in the permittivity in ferroelectric materials corresponds to the Curie temperature (T_C), the transition between the polar and non-polar phases. Meanwhile, in relaxor-like materials, the dielectric peak is not associated with a phase transition but instead shows a permittivity that is frequency-dependent and spreads over a broad temperature range.

Among the analyzed compositions, 80/20 had the highest T_C, above the melting point (at ~150°C), while the relative permittivity amplitude at the peak maximum is the lowest. The highest dielectric permittivity at room temperature was measured in CFE.

Obtained results in Fig. 3b show that in compositions with the amount of TrFE < 30%, the dielectric peak position is fixed within 1 °C around the same temperature, whatever the frequency of measurements. This observation is typical of a classical ferroelectric behavior with a fixed Curie transition temperature. In compositions 55/45 and CFE there is a frequency dispersion in the peak temperature position suggesting a relaxor-like behavior. However, the frequency dispersion does not follow a straight line as it should according to the Vogel-Fulcher (VF) relationship, which was observed in 65/35 gamma-irradiated samples [25]. This irradiation is known to induce a relaxor state by forming irradiation-induced polar defects which have a similar chain-interspacing increase as adding CFE or TrFE to the PVDF [7]. It is worth mentioning that the presence of the amorphous phase and/or its interface with the crystallites (Fig. 2) can also contribute to the dielectric frequency behavior altering the total dielectric response.

The transition from ferroelectric, which is the pristine PVDF and the compositions up to 70/30, to relaxor-like, which are the high-TrFE and CFE systems, is related to the increase in the interchain distance. Simulations in ref. [7] show that with increasing interchain distance, the correlation length of the dipoles is decreasing, causing the dipoles to rotate more easily in the more spacious regions and even to be more susceptible to thermal fluctuations, resulting in the formation of polar clusters or nanodomains. These polar nanodomains are at the origin of frequency dispersion of the maximum dielectric permittivity [26]. Pramanick et al. [27], further suggest that the relaxor behavior in terpolymers is also largely influenced by entanglement and complex interplay between the crystalline and amorphous phases.

The investigated compositions exhibit a peak in dielectric response from room temperature to 140 °C. This behavior not only defines the working region of these materials but is also expected to dramatically influence the functional response of these materials, which we will elaborate on in the next paragraphs.

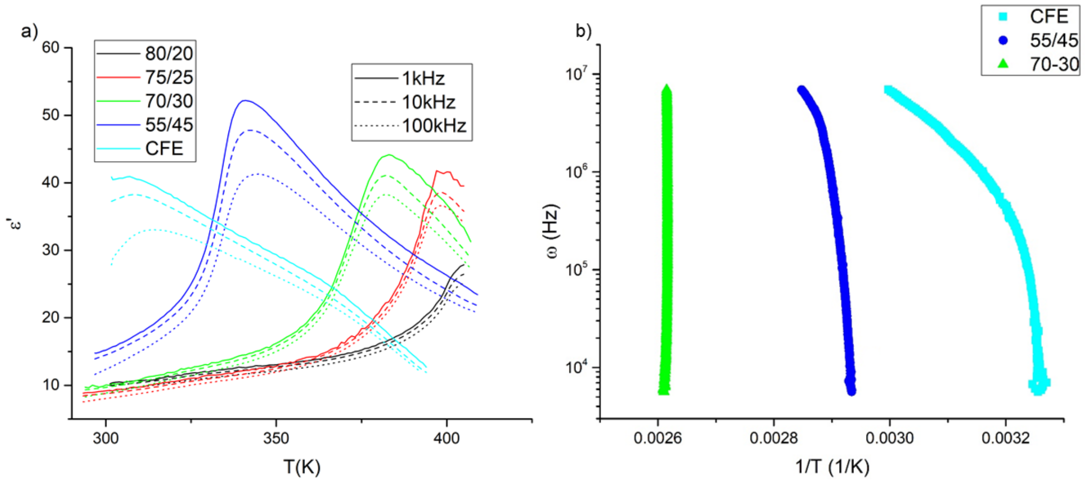

Figure 3. The dielectric response of five PVDF-based materials. a) the real part of the permittivity (ε') versus temperature for all the compositions at different frequencies. b) the logarithm of angular frequency ($\omega=2\pi f$ where f is the frequency) as a function of the inverse of the peak temperature ($1/T_C$).

3.3. Piezoelectric energy harvesting

In this section we highlighted the structural, microstructural and dielectric features of each composition, we focus on the functional response and the functional peculiarities that the different compositions exhibit. The direct piezoelectric effect is one of the key parameters that define the energy output of the energy harvesters. The values of direct effective longitudinal piezoelectric coefficient (d_{33}) measured on the compositions are given in Fig. 4a. The highest d_{33} value was observed in 55/45 (-21 pC/N), while no response was measured in the CFE. In the ferroelectric compositions 80/20, 75/25, and 70/30, d_{33} increases with the content of TrFE until reaching a peak value at 55/45. The microscopic mechanism behind the increased d_{33} at this content of TrFE is interconnected and three-fold. First, the permittivity anomaly is close to room temperature (see Fig. 3a), which signals the high mobility of domain walls and dipoles. Second, the decreased interchain distance (see Fig. 1a&b) additionally eases the switching. Third, the vicinity of the morphotropic phase boundary (MPB, located at ~50% TrFE) provides a flattened energy landscape favorable for enhanced responses.

In terms of maximizing the piezoelectric response, piezoelectric coefficients are not the only essential term [28]. The piezoelectric energy harvesting figure of merit (FOM_{piezo}) is a ratio between the square of the piezoelectric response (d_{33}) over the relative permittivity (ε_{33}). The figure of merit for the the off-resonance piezoelectric response FOM_{piezo} [29] is:

$$FOM_{piezo} = \frac{d_{33}^2}{\varepsilon'_{33}}. \qquad (1)$$

The 70/30 composition has the highest FOM_{piezo} despite the highest d_{33} measured in 55/45 (Fig. 4b), since the permittivity, due to the proximity of the dielectric anomaly (see Fig. 1b), is high in 55/45. It implies that the proximity of phase transitions/anomalies, where the losses are maximized, is not the optimal operating region for energy harvesters. As both d_{33} and ε_{33} depend on the temperature, FOM_{piezo} vs. T plots would precisely define the optimal working region of a specific material.

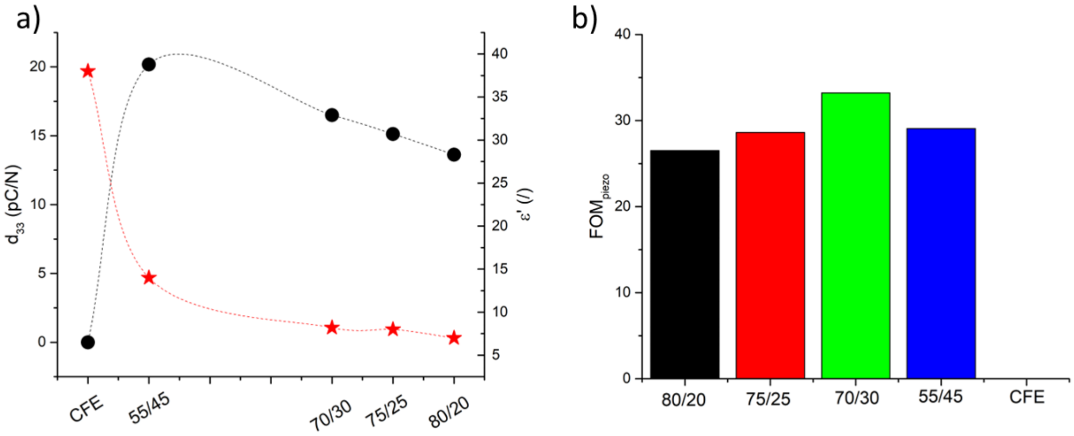

Figure 4. The dielectric and piezoelectric performance of the PVDF-based materials at room temperature. a) piezoelectric and dielectric response and dielectric constant of different compositions. b) piezoelectric off-resonance figure of merit calculated for room temperature.

3.4. Pyroelectric energy harvesting

A discussion about pyroelectric energy harvesting naturally follows that of piezoelectric energy harvesting. All the samples were subjected to a variation in temperature to determine the pyroelectric current and pyroelectric coefficient (*p*). The pyroelectric currents of each composition are given in Fig. 5a. The pyroelectric current is the largest in the 55/45 sample, which was expected since it has the transition temperature the closest to room temperature and the pyroelectric coefficient is paximum at Tc. With decreasing the content of TrFE, the pyroactivity decreased, while the pyroelectric current (not shown) is on the noise level in the CFE composition.

p values were calculated and are shown in Fig. 5b. They range from 21.4 μC/m^{2}K for 55/45 to 10.6 μC/m^{2}K for 80/20. Values obtained for the 80/20 sample are comparable with pure PVDF away from the onset of the Curie transition [30,31]. Not only p is needed to benchmark the compositions in terms of maximal energy output. Indeed, Sebald et al. [32] defined the figure of merit (FOM_{pyro}) for integrating materials into pyroelectric energy harvesters as:

$$FOM_{pyro} = \frac{p^2}{\varepsilon'_r}, \qquad (2)$$

where ε'_r is the relative permittivity, and p is the pyroelectric constant. The FOM_{pyro} for the studied compositions are given in Fig. 5b. 70/30 is again the dominant material due to its high p and low permittivity relative to the other compositions.

It should be stressed that the figure of merit used here does not include the heat transport properties, which are also of key importance because they define the rate at which the temperature can be varied. It follows that this rate defines the amount of energy that can be generated with pyroelectric energy harvesting [33]. Highly textured composites with anisotropic thermal transport properties should be designed and fabricated to maximize further the response of the pyroelectric harvesting materials [34,35].

The results also imply that working near the transition temperature is not necessarily optimal due to the *FOM*$_{\text{pyro}}$, which is related to the ratio between the pyroelectric coefficient and the dielectric permittivity, as both drastically increase near the transition.

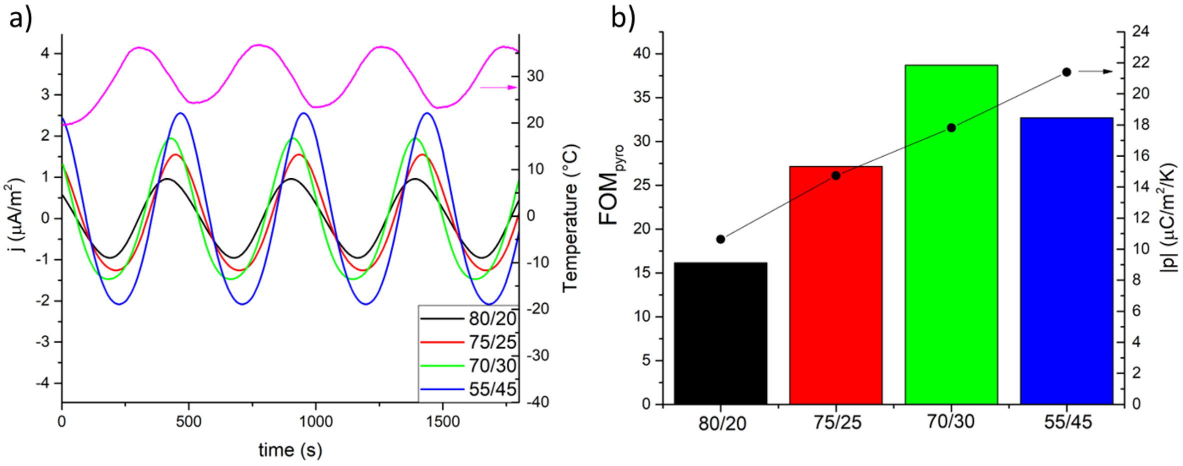

Figure 5. Pyroelectric effect of the P(VDF-TrFE). a) the pyroelectric current density generated by the different compositions. b) the pyroelectric figure of merit calculated for the analyzed compositions (FOM$_{\text{pyro}}$) and on the right axis the pyroelectric coefficient (p).

3.5. Triboelectric energy harvesting

A relatively novel method of energy harvesting from the environment is triboelectricity. The triboelectric effect has been known for centuries, but only recently it was shown that its uses in harvesting applications are interesting [17]. The underlying mechanism is not well-understood; in general, the effect occurs in two steps: contact electrification followed by electrostatic induction [36,37]. Contact electrification happens when two surfaces/materials come in close contact and exchange electrons due to different work functions. When the contact is separated, the surface charges are compensated by the electrostatic induction phenomenon. The charge redistribution during the compensation is responsible for the electric output work.

The force applied to the samples and the triboelectric voltages (U_{tribo}) generated by the samples is shown in Fig. 6a.

The peak voltages ranged from -36 V for 55/45 to ~0 V for CFE. One voltage peak appears just after the contact, as shown in Fig. 6a (see force and voltage peaks). The contact time is denoted by a dashed line and numbered 1. The separation time is again denoted by a dashed line and numbered 2, where another voltage peak is observed right after. Some more minor voltage variations were observed, most probably due to the non-equal distribution of the forces due to the non-perfect alignment of the sample and the aluminum side. It is also interesting to note that the voltage converged to a final value after a certain amount of time (cycles). The possible explanation for this is gradual migration of the defect ions [38] or surface poling of the material itself due to the electrostatic forces created.

Defining the figure of merit for triboelectric materials is difficult because the phenomenon is related to the electronic structure of the dielectric and metal in contact. Nonetheless, some figures of merit have been proposed [37,39]. The figure of merit that best describes triboelectric energy harvesting is [39]:

$$FOM_{tribo} = \frac{\sigma^2}{\varepsilon_0} \qquad (3)$$

σ is the generated surface charges of the surface under investigation and ε_0 is the dielectric permittivity of vacuum.

However, since σ is challenging to determine, we used the root mean square of the voltage signal ($U_{\mathrm{OC\text{-}RMS}}$) as the figure of merit. This factor is proportional to the power output since all the samples are connected to the same resistance (R of 100 MΩ in Fig. 6b) value. Interestingly, the values of the power (seen in Fig. 6c) extracted by the triboelectric experiment to some degree correlate with the FOM_{piezo} (see Fig. 4b). This implies that similar mechanisms drive the triboelectric effect in (relaxor-)ferroelectric compositions. We assume effects are related to the degree of (spontaneous) polarization, as already shown in some articles [40], and to the dielectric permittivity of the materials. It is also possible that during the triboelectric cycling, the surface region was self-poled by the charged surface and the migration of point defects, which means that a part of the contribution to the generated voltage was from the piezoelectric effect. The oscillation of the voltage during the contact phase (between 1 and 2 in Fig. 6c), which seems to directly correlate with the oscillation of pressure would support the idea of self-poled regions and piezoelectric response since the generated voltage is negative when under pressure which is expected from the piezoelectric response with a negative d_{33}. It is therefore not excluded that here some piezoelectric effect also contributes to the total triboelectric response, as well as other mechanisms such as electrostriction and flexoelectricity.

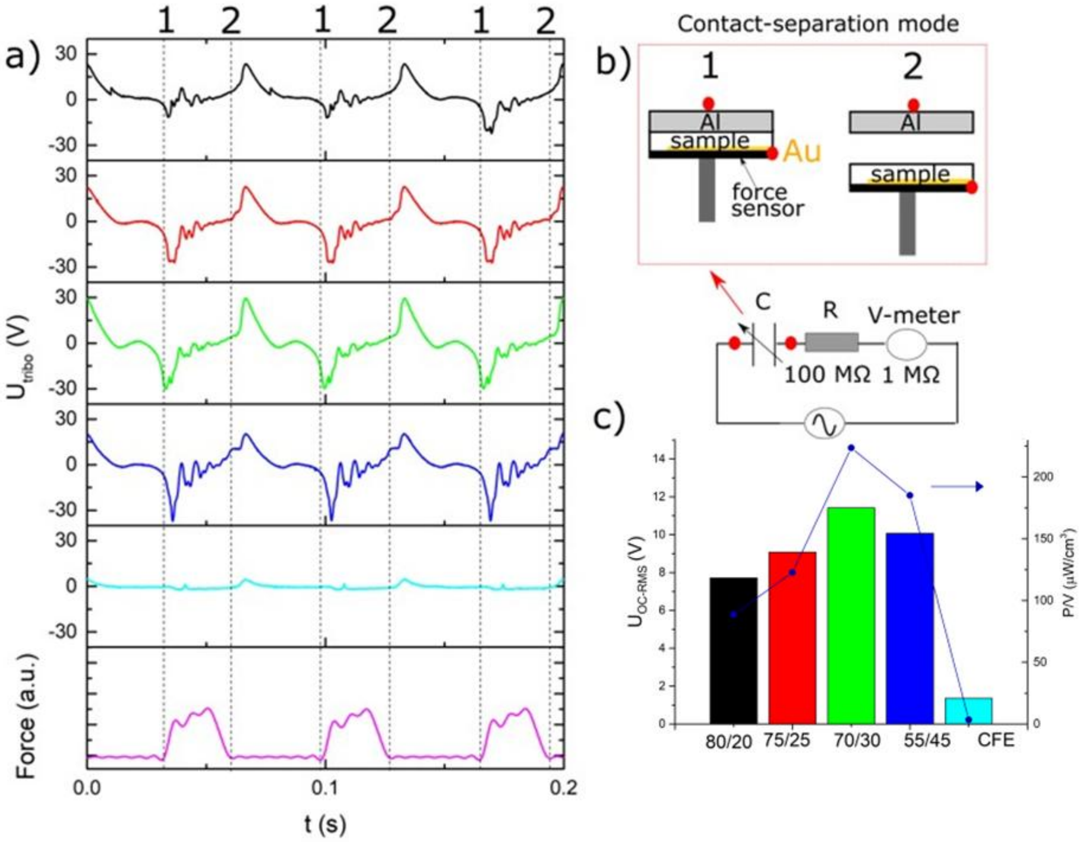

Figure 6. Triboelectric energy harvesting at room temperature. a) force applied to the samples and voltage (U_{tribo}) generated by the triboelectric contact-separation mode for different compositions as a function of time. b) Schematic illustration of the measuring setup. c) the root-mean-square voltage (U_{OC-RMS}) and power values extracted from the triboelectric cycling.

3.6. Energy storage

Energy generated by the three energy harvesting methods, piezoelectric, pyroelectric, and triboelectric must now be effectively stored. It was considered whether the same compositions that generated the energy could be used to store the energy until it is supplied to the consumer. PVDF-based materials were recently shown to possess high storage capability [21].

The energy storage properties were calculated from unipolar loops shown in Fig. 7a. The polarization values at the maximal field are the largest in the CFE composition and the smallest in the 80/20. The latter reflects the short- and long-range order, respectively. While the dipoles in 80/20 were permanently oriented with poling, as for classical ferroelectrics, CFE possesses randomly oriented dipoles aligned only under the applied electric field [41]. The energy storage at depolarization was evaluated from the polarization values. In contrast to the trends of the harvesting methods, the energy storage is minimal for 80/20 and increases with increasing the TrFE amount and is the highest in CFE with 1.52 J/cm^3 (see Fig. 7b) Although the stored power for 55/45 is higher than for the other copolymers, its efficiency is much lower, possibly due to the relaxor-to-ferroelectric phase transitions.

The values are in general comparable to some well-known energy storage materials such as antiferroelectric $NaNbO_3$-based materials [42], owing mainly to the larger breakdown field of PVDF-based materials.

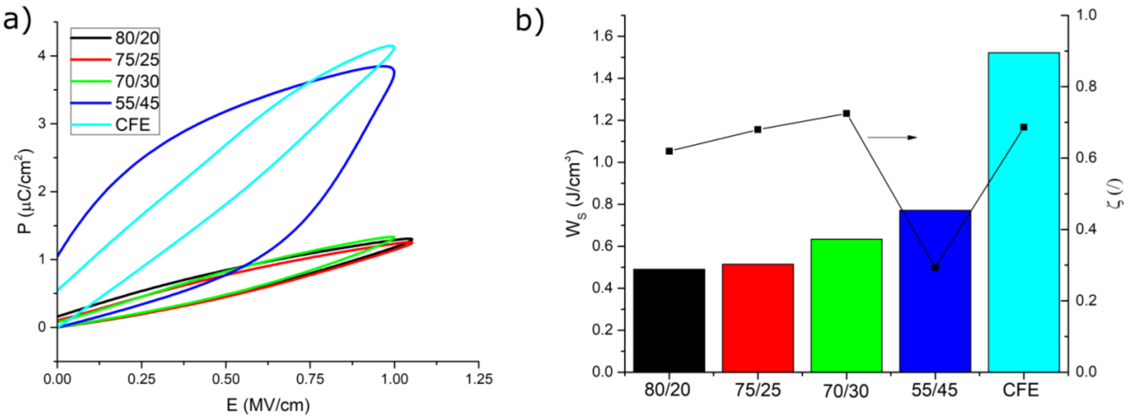

Figure 7. Energy storage and efficiency calculated at room temperature. a) unipolar polarization-electric field (P-E) loops measured at room temperature and 20 Hz with the field magnitude of 1 MV/cm. b) the calculated energy storage density (W_S) and storage efficiency (ζ). Discharge values.

3.7. **Summary and conclusions**

Within this study, we try to promote the agenda that showing merely the conversion coefficients does not provide sufficient information in the selection process for materials for energy harvesting. The so-called figures of merit are more informative and give a more straightforward answer because they are proportional to the energy output.

A radar plot was utilized (Fig. 8a) to summarize this study findings and to find the best all-around composition. The radar plot was used to plot the FOM_{piezo}, FOM_{pyro}, $U_{\mathrm{RMS\text{-}OC}}$, and $W_{\mathrm{S}}{\cdot}\zeta$ normalized to the highest value obtained in the specific section (FOM_{piezo}: 70/30, FOM_{pyro}: 70/30, $U_{\mathrm{RMS\text{-}OC}}$: 70/30, $W_{\mathrm{S}}{\cdot}\zeta$: CFE).

For each composition, the area defined by these four parameters was then evaluated and normalized again to the highest area obtained amongst the compositions. In our case, this was for 70/30. Fig. 8b indicates the best all-around material (70/30, area is by definition 100%) and how much the followers are behind the optimal composition. It can be seen from Fig. 8b, that 70/30 is leading when considering all four sections. The 70/30 is the best all-around material, leading in all three harvesting categories. However, its long-range ferroelectric order with remanent polarization prevents high energy storage capabilities since the polarization change with the application of electric field is relatively low compared to relaxor CFE. It seems that 70/30 is an optimal choice in terms of material responsivity, which is tuned by varying the interchain distance of the material. The CFE composition has superior energy storage capability, while its relaxor-like nature prevents it from having high piezo-, pyro-, tribo- electric responses.

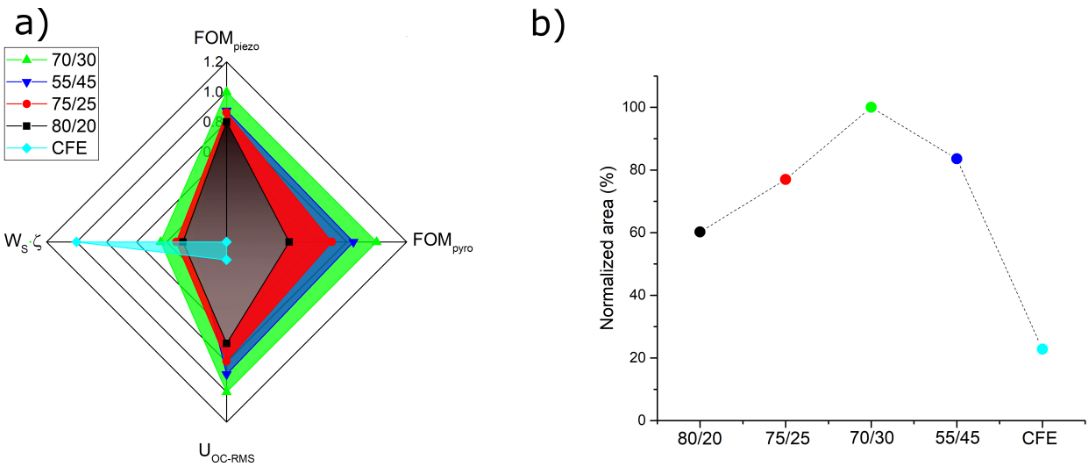

Figure 8. The final benchmarking of the samples. a) a radar plot of the four normalized parameters, which help determine the best all-for-one material. b) the areas calculated from a) and normalized on the largest area, which was 80/20. The dashed line is a guide to the eyes.

Acknowledgments

The authors acknowledge the “Investissements d’Avenir” program (ANR-10-LABX-0035, LabexNanoSaclay through the flagship NanoVibes), PHC Slovenian-French Proteus mobility grant (BI-FR/21-22-PROTEUS-004), Slovenian Research Agency (program P2-0105), ARRS (Slovenian research agency) J2-2508, and FNR-Luxembourg INTERmobility grant (INTER/Mobility/19/13992074).

4. References

(1) Jaffe, B.; Cook, W. R. J.; Jaffe, H. L. *Piezoelectric Ceramics*; Roberts, J. P., Popper, P., Eds.; Academic Press Inc.: London, United Kingdom, 1971; Vol. 3.

(2) Awolusi, I.; Marks, E.; Hallowell, M. Wearable Technology for Personalized Construction Safety Monitoring and Trending: Review of Applicable Devices. *Autom. Constr.* **2018**, *85* (July 2016), 96–106. https://doi.org/10.1016/j.autcon.2017.10.010.

(3) Taraldsen, K.; Chastin, S. F. M.; Riphagen, I. I.; Vereijken, B.; Helbostad, J. L. Physical Activity Monitoring by Use of Accelerometer-Based Body-Worn Sensors in Older Adults: A Systematic Literature Review of Current Knowledge and Applications. *Maturitas* **2012**, *71* (1), 13–19. https://doi.org/10.1016/j.maturitas.2011.11.003.

(4) Chen, X.; Han, X.; Shen, Q. D. PVDF-Based Ferroelectric Polymers in Modern Flexible Electronics. *Adv. Electron. Mater.* **2017**, *3* (5). https://doi.org/10.1002/aelm.201600460.

(5) Lovinger, A. J. Poly(Vinylidene Fluoride). In *Developments in Crystalline Polymers—1*; Springer Netherlands: Dordrecht, 1982; Vol. 4, pp 195–273. https://doi.org/10.1007/978-94-009-7343-5_5.

(6) Furukawa, T. Structure and Properties of Ferroelectric Polymers. *Mech. Corros. Prop. Ser. A, Key Eng. Mater.* **1994**, *92–93* (97), 15–30. https://doi.org/10.4028/www.scientific.net/kem.92-93.15.

(7) Yang, L.; Li, X.; Allahyarov, E.; Taylor, P. L.; Zhang, Q. M.; Zhu, L. Novel Polymer Ferroelectric Behavior via Crystal Isomorphism and the Nanoconfinement Effect. *Polymer (Guildf).* **2013**, *54* (7), 1709–1728. https://doi.org/10.1016/j.polymer.2013.01.035.

(8) Meng, Y.; Zhang, Z.; Wu, H.; Wu, R.; Wu, J.; Wang, H.; Pei, Q. A Cascade Electrocaloric Cooling Device for Large Temperature Lift. *Nat. Energy* **2020**, *5* (12), 996–1002. https://doi.org/10.1038/s41560-020-00715-3.

(9) Tian, B.; Liu, L.; Yan, M.; Wang, J.; Zhao, Q.; Zhong, N.; Xiang, P.; Sun, L.; Peng, H.; Shen, H.; Lin, T.; Dkhil, B.; Meng, X.; Chu, J.; Tang, X.; Duan, C. A Robust Artificial Synapse Based on Organic Ferroelectric Polymer. *Adv. Electron. Mater.* **2019**, *5* (1), 1–8. https://doi.org/10.1002/aelm.201800600.

(10) Lheritier, P.; Noel, S.; Vaxelaire, N.; Domingues Dos Santos, F.; Defay, E. Actuation Efficiency of Polyvinylidene Fluoride-Based Co- and Ter-Polymers. *Polymer (Guildf).* **2018**, *156* (May), 270–275. https://doi.org/10.1016/j.polymer.2018.10.003.

(11) Maity, K.; Garain, S.; Henkel, K.; Schmeißer, D.; Mandal, D. Self-Powered Human-Health Monitoring through Aligned PVDF Nanofibers Interfaced Skin-Interactive Piezoelectric Sensor. *ACS Appl. Polym. Mater.* **2020**, *2* (2), 862–878. https://doi.org/10.1021/acsapm.9b00846.

(12) Costa, P.; Nunes-Pereira, J.; Pereira, N.; Castro, N.; Gonçalves, S.; Lanceros-Mendez, S. Recent Progress on Piezoelectric, Pyroelectric, and Magnetoelectric Polymer-Based Energy-Harvesting Devices. *Energy Technol.* **2019**, *7* (7), 1–19. https://doi.org/10.1002/ente.201800852.

(13) Yang, Z.; Zhou, S.; Zu, J.; Inman, D. High-Performance Piezoelectric Energy Harvesters and Their Applications. *Joule* **2018**, *2* (4), 642–697. https://doi.org/10.1016/j.joule.2018.03.011.

(14) Bhalla, A. S.; Newnham, R. E. Primary and Secondary Pyroelectricity. *Phys. Status Solidi* **1980**, *58* (1), K19–K24. https://doi.org/10.1002/pssa.2210580146.

(15) Bowen, C. R.; Taylor, J.; Leboulbar, E.; Zabek, D.; Chauhan, A.; Vaish, R. Pyroelectric Materials and Devices for Energy Harvesting Applications. *Energy Environ. Sci.* **2014**, *7* (12), 3836–3856. https://doi.org/10.1039/c4ee01759e.

(16) Zhao, T.; Jiang, W.; Niu, D.; Liu, H.; Chen, B.; Shi, Y.; Yin, L.; Lu, B. Flexible Pyroelectric Device for Scavenging Thermal Energy from Chemical Process and as Self-Powered Temperature Monitor. *Appl. Energy* **2017**, *195*, 754–760. https://doi.org/10.1016/j.apenergy.2017.03.097.

(17) Fan, F. R.; Tian, Z. Q.; Lin Wang, Z. Flexible Triboelectric Generator. *Nano Energy* **2012**, *1* (2), 328–334. https://doi.org/10.1016/j.nanoen.2012.01.004.

(18) Liu, Y.; Tian, G.; Wang, Y.; Lin, J.; Zhang, Q.; Hofmann, H. F. Active Piezoelectric Energy Harvesting: General Principle and Experimental Demonstration. *J. Intell. Mater. Syst. Struct.* **2009**, *20* (5), 575–585. https://doi.org/10.1177/1045389X08098195.

(19) Liang, J.; Liao, W. H. Energy Flow in Piezoelectric Energy Harvesting Systems. *Smart Mater. Struct.* **2011**, *20* (1). https://doi.org/10.1088/0964-1726/20/1/015005.

(20) Chu, B. A Dielectric Polymer with High Electric Energy Density and Fast Discharge Speed. *Science (80-.).* **2006**, *313* (5785), 334–336. https://doi.org/10.1126/science.1127798.

(21) Liu, Y.; Lin, Y.-T.; Haibibu, A.; Xu, W.; Zhou, Y.; Li, L.; Kim, S. H.; Wang, Q. Relaxor Ferroelectric Polymers: Insight into High Electrical Energy Storage Properties from a Molecular Perspective. *Small Sci.* **2021**, *1* (3), 2000061. https://doi.org/10.1002/smsc.202000061.

(22) Jiang, H.; Yang, J.; Xu, F.; Wang, Q.; Liu, W.; Chen, Q.; Wang, C.; Zhang, X.; Zhu, G. VDF-Content-Guided Selection of Piezoelectric P(VDF-TrFE) Films in Sensing and Energy Harvesting Applications. *Energy Convers. Manag.* **2020**, *211* (March), 112771. https://doi.org/10.1016/j.enconman.2020.112771.

(23) Bai, Y.; Jantunen, H.; Juuti, J. Energy Harvesting Research: The Road from Single Source to Multisource. *Adv. Mater.* **2018**, *30* (34), 1–41. https://doi.org/10.1002/adma.201707271.

(24) Lovinger, A. J.; Furukawa, T.; Davis, G. T.; Broadhurst, M. G.; Furukawa, T. Crystalline Forms in a Copolymer of Vinylidene Fluoride and Trifluoroethylene (52/48 Mol %).

Macromolecules **1982**, *15* (2), 323–328. https://doi.org/10.1021/ma00230a024.

(25) Casar, G.; Li, X.; Koruza, J.; Zhang, Q.; Bobnar, V. Electrical and Thermal Properties of Vinylidene Fluoride-Trifluoroethylene- Based Polymer System with Coexisting Ferroelectric and Relaxor States. *J. Mater. Sci.* **2013**, *48* (22), 7920–7926. https://doi.org/10.1007/s10853-013-7602-4.

(26) Cross, L. E. Relaxor Ferroelectrics. *Ferroelectrics* **1987**, *76* (1), 241–267. https://doi.org/10.1080/00150198708016945.

(27) Pramanick, A.; Osti, N. C.; Jalarvo, N.; Misture, S. T.; Diallo, S. O.; Mamontov, E.; Luo, Y.; Keum, J. K.; Littrell, K. Origin of Dielectric Relaxor Behavior in PVDF-Based Copolymer and Terpolymer Films. *AIP Adv.* **2018**, *8* (4). https://doi.org/10.1063/1.5014992.

(28) Roscow, J. I.; Pearce, H.; Khanbareh, H.; Kar-Narayan, S.; Bowen, C. R. Modified Energy Harvesting Figures of Merit for Stress- and Strain-Driven Piezoelectric Systems. *Eur. Phys. J. Spec. Top.* **2019**, *228* (7), 1537–1554. https://doi.org/10.1140/epjst/e2019-800143-7.

(29) Priya, S. Criterion for Material Selection in Design of Bulk Piezoelectric Energy Harvesters. *IEEE Trans. Ultrason. Ferroelectr. Freq. Control* **2010**, *57* (12), 2610–2612. https://doi.org/10.1109/TUFFC.2010.1734.

(30) Burkard, H.; Pfister, G. Reversible Pyroelectricity and Inverse Piezoelectricity in Polyvinylidene Fluoride. *J. Appl. Phys.* **1974**, *45* (8), 3360–3364. https://doi.org/10.1063/1.1663785.

(31) Sagar, R.; Gaur, S. S.; Gaur, M. S. Effect of BaZrO3 Nanoparticles on Pyroelectric Properties of Polyvinylidene Fluoride (PVDF). *J. Therm. Anal. Calorim.* **2017**, *128* (2), 1235–1239. https://doi.org/10.1007/s10973-016-5964-y.

(32) Sebald, G.; Seveyrat, L.; Guyomar, D.; Lebrun, L.; Guiffard, B.; Pruvost, S. Electrocaloric and Pyroelectric Properties of 0.75Pb(Mg 1/3Nb2/3)O3-0.25PbTiO3 Single Crystals. *J. Appl. Phys.* **2006**, *100* (12), 0–6. https://doi.org/10.1063/1.2407271.

(33) Pandya, S.; Velarde, G.; Zhang, L.; Wilbur, J. D.; Smith, A.; Hanrahan, B.; Dames, C.; Martin, L. W. New Approach to Waste-Heat Energy Harvesting: Pyroelectric Energy Conversion. *NPG Asia Mater.* **2019**, *11* (1). https://doi.org/10.1038/s41427-019-0125-y.

(34) Yan, J.; Liu, M.; Jeong, Y. G.; Kang, W.; Li, L.; Zhao, Y.; Deng, N.; Cheng, B.; Yang, G. Performance Enhancements in Poly(Vinylidene Fluoride)-Based Piezoelectric Nanogenerators for Efficient Energy Harvesting. *Nano Energy* **2019**, *56* (December 2018), 662–692. https://doi.org/10.1016/j.nanoen.2018.12.010.

(35) Anand, A.; Bhatnagar, M. C. Effect of Sodium Niobate (NaNbO3) Nanorods on β-Phase Enhancement in Polyvinylidene Fluoride (PVDF) Polymer. *Mater. Res. Express* **2019**, *6* (5), 55011. https://doi.org/10.1088/2053-1591/aaefd9.

(36) Wang, Z. L.; Wang, A. C. On the Origin of Contact-Electrification. *Mater. Today* **2019**,

30 (November), 34–51. https://doi.org/10.1016/j.mattod.2019.05.016.

(37) Wu, C.; Wang, A. C.; Ding, W.; Guo, H.; Wang, Z. L. Triboelectric Nanogenerator: A Foundation of the Energy for the New Era. *Adv. Energy Mater.* **2019**, *9* (1), 1–25. https://doi.org/10.1002/aenm.201802906.

(38) MacKey, M.; Schuele, D. E.; Zhu, L.; Baer, E. Layer Confinement Effect on Charge Migration in Polycarbonate/ Poly(Vinylidene Fluorid-Co-Hexafluoropropylene) Multilayered Films. *J. Appl. Phys.* **2012**, *111* (11). https://doi.org/10.1063/1.4722348.

(39) Peng, J.; Kang, S. D.; Snyder, G. J. Optimization Principles and the Figure of Merit for Triboelectric Generators. *Sci. Adv.* **2017**, *3* (12), 1–7. https://doi.org/10.1126/sciadv.aap8576.

(40) Bai, P.; Zhu, G.; Zhou, Y. S.; Wang, S.; Ma, J.; Zhang, G.; Wang, Z. L. Dipole-Moment-Induced Effect on Contact Electrification for Triboelectric Nanogenerators. *Nano Res.* **2014**, *7* (7), 990–997. https://doi.org/10.1007/s12274-014-0461-8.

(41) Jin, L.; Li, F.; Zhang, S. Decoding the Fingerprint of Ferroelectric Loops: Comprehension of the Material Properties and Structures. *J. Am. Ceram. Soc.* **2014**, *97* (1), 1–27. https://doi.org/10.1111/jace.12773.

(42) Fulanović, L.; Zhang, M. H.; Fu, Y.; Koruza, J.; Rödel, J. NaNbO3-Based Antiferroelectric Multilayer Ceramic Capacitors for Energy Storage Applications. *J. Eur. Ceram. Soc.* **2021**, *41* (11), 5519–5525. https://doi.org/10.1016/j.jeurceramsoc.2021.04.052.